The impact of Mg^{2+} ions on equilibration of Mg-Ca carbonates in groundwater and brines

Peter Möller[a,*] Marco De Lucia[a]

[a]Helmholtz Centre Potsdam, GFZ German Research for Geosciences
Section 3.4 Fluid Systems Modelling, Telegrafenberg, 14473 Potsdam, Germany

*Corresponding author, pemoe@gfz-potsdam.de, tel: +49 331 288 1430

Preprint compiled on 2019/07/04 at 15:57:23

Abstract

At temperatures below 50 °C, the Mg^{2+}/Ca^{2+} values in groundwater and brines, irrespective of their origin - either carbonaceous or siliceous rocks/sediments - show a large spread. As shown by equilibria of surface layer composition of calcite in solutions containing Mg^{2+}, $\log_{10}({}^{a}Mg^{2+}/{}^{a}Ca^{2+})$ vary between minus infinity and +2.3, thereby covering thermodynamical equilibria between the minerals calcite, aragonite, dolomite and huntite. $Log_{10}({}^{a}Mg^{2+}/{}^{a}Ca^{2+})$ in solution of dissolving ordered dolomite at 25 °C fits the thermodynamical equilibrium between disordered dolomite and calcite and nearly corresponds to that of pure calcite with a dolomitic surface layer due to exchange of Ca^{2+} against Mg^{2+} in Mg^{2+}-containing solutions. This observation suggests that the solubility of Mg-Ca carbonates is controlled by the composition of their monomolecular surface layers in equilibrium with the ambient aqueous phase. Incongruently dissolving minerals such as dolomite attain equilibrium between individual surface compositions of different carbonates. The bulk composition of these carbonates never equilibrates with the ambient solution due to extremely low ion mobility in the lattice. However, the thermodynamical equilibria are usually based on the composition of bulk minerals, therefore their estimates of equilibria between carbonates, i.e., $\log_{10}({}^{a}Mg^{2+}/{}^{a}Ca^{2+})$ in solution, differ significantly from values established by the chemical composition and structure of the surface layer of carbonates.

1 Introduction

Besides hydrated metastable phases, a wide variation in composition of Mg-Ca carbonates occurs in nature between the possible endmembers calcite and magnesite (Table 1). Low magnesian calcite (LMC) precipitates inorganically, whereas high magnesian calcite (HMC) is either of biogenic or diagenetic origin. Nesquehonite but not magnesite forms at ambient temperatures (Davies and Bubela, 1973; Zachmann et al., 1989) (Table 1). The experimental formation of dolomite below temperatures of about 50 °C is impeded by kinetics because of lacking the necessary activation energy needed for fully dehydration of Mg^{2+} in dolomite nuclei (Gregg and Sibley, 1984; Land, 1998; Arvidson et al., 1999; Mavromatis et al., 2013; Baldermann et al., 2015; Wang et al., 2016; Perez-Fernandez et al., 2017). Alternatively, the inhibited growth of dolomite is explained by deposition of a "poorly ordered dolomite-like phase that poisons the surface" (Berninger et al., 2017). In nature, however, dolomite seemingly forms below 50 °C but its formation is not fully understood yet (Gregg et al., 2014). Although HMC and VHMC/proto-dolomite (Table 1) are metastable, they are known to survive geological times (Land, 1985).

Mineral	**Abbr.**	**Composition**	**mol-%** $MgCO_3$
Calcite		$CaCO_3$	0
Aragonite		$CaCO_3$	0
Low Mg calcite	LMC	$Ca_yMg_{(1-y)}CO_3$	<4
High Mg calcite	HMC	$Ca_yMg_{(1-y)}CO_3$	4-30
Very high Mg calcite	VHMC	$Ca_yMg_{(1-y)}CO_3$	30-45
Disordered dolomite		$Ca_xMg_{(2-x)}(CO_3)_2$	46-50
= proto dolomite			
Ordered dolomite		$Ca_xMg_{(2-x)}(CO_3)_2$	46-50
Huntite		$CaMg_3(CO_3)_4$	75
Nesquehonite		$MgCO_3 * 3H_2O$	100
Hydromagnesite		$Mg_5[OH/(CO_3)_2]_2$	100
Magnesite		$MgCO_3$	100

Table 1: *Ca-Mg carbonates, their chemical formula and the mol-%* $MgCO_3$*. The subscripts* x *and* y *express the deviation from the stoichiometric coefficients of endmembers calcite and dolomite, respectively; both are one for the perfectly stoichiometric phases.*

These metastable products occur side by side together with ordered dolomite without establishing bulk equilibria (Brätter et al., 1972; Warren, 2000). The Mg^{2+} concentrations inhibit growth of calcite by increasing its solubility due to incorporation of Mg^{2+} into the calcite lattice (Plummer and Mackenzie, 1974; Thorstenson and Plummer, 1977; Mucci and Morse, 1983; Davis et al., 2000). The exchange of Mg^{2+} against Ca^{2+} in calcite surface layers leads to an increase of calcite solubility (Koss and Möller, 1974). This process is reviewed in subsection 3.1 because it constitutes the base for the critical review of solubility of Mg-Ca carbonates in general. Under increased activities of Mg^{2+} and Ca^{2+} in solution, also aragonite precipitates (Kitano et al., 1962). The calcite growth rate decreased in presence of Mg^{2+} and SO_4^{2-} (Prokovsky and Schott, 2001; Prokovsky et al., 2005, 2009a,b; Gledhill and Morse, 2006; Nielsen et al., 2016), which both enhances the hydrophilic character of the calcite surface and weakens the adsorption of organic compounds (Generosi et al., 2016; Andersson et al., 2016). Besides inorganic components, also organic components inhibit growth of calcite such as citrate (Montanari et al., 2017), alginate (Lakstanov et al., 2017) and acetate (Dobberschütz et al., 2018).

The aim of this contribution is to decipher the conditions under which differently composed Mg-Ca carbonates equilibrate in aqueous solutions. An answer is approached by comparing thermodynamically and analytically derived ratios of Mg^{2+} and Ca2+ in ambient solutions of calcite and dolomite.

2 Thermodynamic approaches to Mg^{2+}/Ca^{2+} at equilibria of carbonates

Thermodynamics suggest that the carbonate equilibria compiled in Table 2 are given by the activity ratio of Mg^{2+} and Ca^{2+} (Equation 1). The activities of the solids are taken as unity. Depending on the thermodynamic data sets different temperature-dependent trends for ordered dolomite-calcite and disordered dolomite-calcite are derived (Figure 1). These equilibria are calculated using the freely available CHNOSZ package (Dick, 2008) which implements both the revised equations for aqueous species and the Berman and Brown (1985) equations for minerals and the revised Helgeson-Kirkham-Flowers's (Helgeson et al., 1981) equations for aqueous species. The equilibrium of various carbonates expressed as $\log_{10}({}^{a}Mg^{2+}/{}^{a}Ca^{2+})$ are

69 therefore based on 3 different thermodynamic databases and their underlying formalisms,

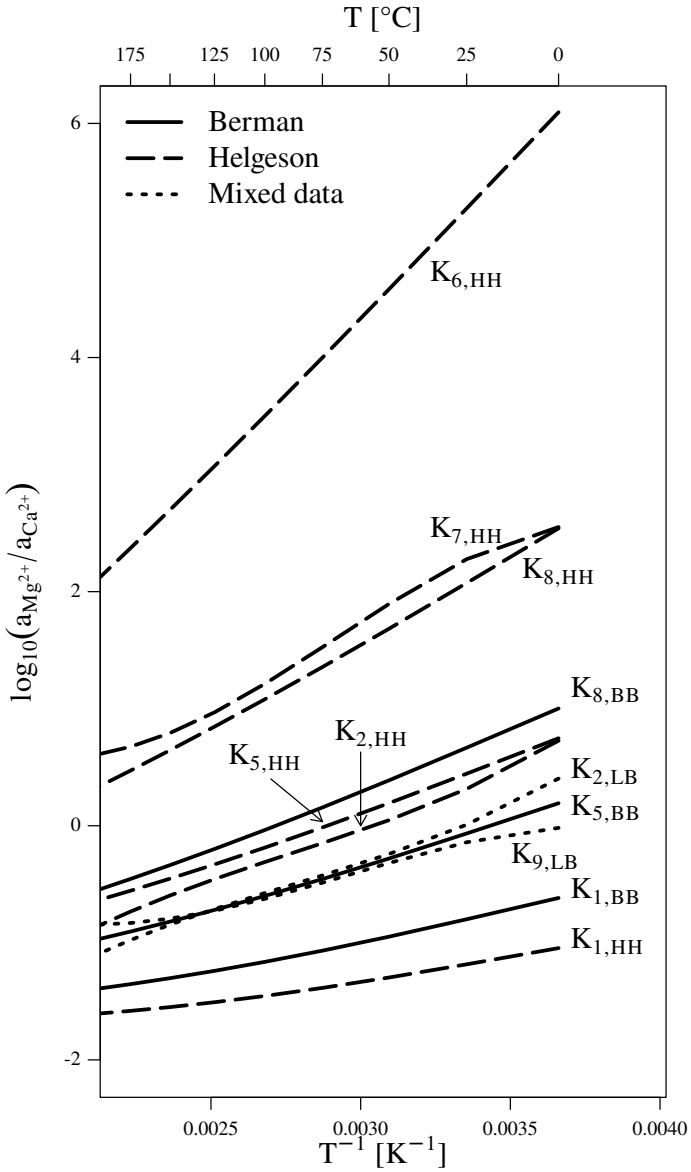

Figure 1: *Thermodynamic estimates of mineral equilibria in the temperature range of 0–175 °C. In the indices of K, the figures refer to the reaction in Table 2; capital letters indicate the sources of thermodynamic data of the educt and product in the corresponding reaction:* BB*, both are from Berman (1988);* HH*, both are from Helgeson et al. (1978);* LB*, data for the educt data are taken from "llnl.dat" data base (Appelo et al., 2014) and the product data from Berman (1988). These line types are used in the following plots.*

70 • the compilations of Berman (1988),

71 • the compilation of Helgeson et al. (1978), of Plummer et al. (1982) and of Berman (1988)
72 with many successive integrations, and

73 • where the necessary data are not available in the above compilations, such as disordered
74 dolomite, data on dissolution of minerals are extracted from the "llnl.dat" database
75 distributed with PHREEQC 3.4.0 (Appelo et al., 2014).

Note that the dissolution reactions $i = 12 - 16$ in Table 3 are needed to evaluate the reaction constant $\log_{10} K_i$ with $i = 2, 4, 7, 9$ and 11 the reactions in which disordered dolomite is involved.

Figure 1 displays the temperature-dependent equilibria of all considered mineral equilibria in Table 2. Note the discrepancies between equilibria based on thermodynamical data of Berman (1988) and those of Helgeson et al. (1978). Since Berman followed chronologically Helgeson et al. (1981) and partially revised their approach, we consider his data most reliable. It has to be noted that mixing data may introduce additional inconsistencies in the calculations.

The equilibrium of the substoichiometrically composed magnesian calcite and dolomite, with the same subscript convention adopted in Table 1, is expressed in Equation 1. $\mathrm{Log_{10}K_{x/y}}$ (Equation 2) is derived from Equation 1. Equation 2 can be developed into Equation 3 in terms of free energy of reaction. The indices x and y indicates the surface phases of dolomite and calcite, respectively.

$$2Ca_yMg_{(1-y)}CO_3 + (2y-x) \cdot Mg^{2+} = Ca_xMg_{(2-x)}(CO_3)_2 + (2y-x) \cdot Ca^{2+} \quad (1)$$

$$\log_{10} K_{x/y} = -(2y-x) \log_{10} \frac{{}^aMg^{2+}}{{}^aCa^{2+}} + \log_{10} \frac{\{{}^a dol_x\}}{\{{}^a Cc_y\}^2} \quad (2)$$

$$\frac{\Delta_r G}{\ln(10) RT} = (2y-x) \log_{10} \frac{{}^aMg^{2+}}{{}^aCa^{2+}} + \log_{10} \frac{\{{}^a Cc_y\}^2}{\{{}^a dol_x\}} \quad (3)$$

The assumption of equilibrium for the reaction of Equation 1 results in Equation 4:

$$\log_{10} \frac{{}^aMg^{2+}}{{}^aCa^{2+}} = \frac{1}{2y-x} \log_{10} \frac{\{{}^a dol_x\}}{\{{}^a Cc_y\}^2} \quad (4)$$

Thus, the activity ratio of Mg^{2+} and Ca^{2+} in solution depends on the stoichiometric factors of magnesian calcite and disordered dolomite and on the activity ratio of the surface phases ${}^a dol_x$ and the square of $\{{}^a Cc_y\}^2$. If $[{}^aMg^{2+}]/[{}^aCa^{2+}]=1$, it follows from Equation 4 that $\{{}^a dol_x\}=\{{}^a Cc_y\}^2$.

3 The impact of Mg^{2+} on calcite solubility

3.1 Summary of past work on Ca^{2+}-Mg^{2+} exchange at calcite surfaces

Distilled water was saturated with respect to reagent grade $CaCO_3$ p.a. (Merck®) or single crystals of calcite for periods of 10 days at temperatures between 20-25 °C and atmospheric pCO_2. The 4 µm filtered calcite-saturated solution was spiked with ^{45}Ca (β-decay with half-life of 163.8 days). The equilibrated calcite was placed in the spiked solution for at least 15 hours, where it underwent ion exchange of $^{45}Ca^{2+}$ against Ca^{2+} in the calcite surface. Thereafter the calcite was separated from its solution, cleaned with distilled water, dried, and the β-activity was determined by low β-proportional counting assembly (Möller and Sastri, 1974; Sastri and Möller, 1974). Thereafter the ^{45}Ca spiked solids were placed into a calcite-saturated solution to which a small amount of $MgCl_2$ was added. After 15 hours the calcite was washed and dried for β counting. This procedure is repeated with increasing amounts of $MgCl_2$ in calcite saturated solutions (Möller and Rajagopalan, 1972; Möller, 1973). In these Mg^{2+} containing solutions calcite underwent exchange of surface Ca^{2+} ions against Mg^{2+} and $^{45}Ca^{2+}$ decreased in the calcite surface. With increasing Mg^{2+}concentrations in solution the Mg^{2+}/Ca^{2+} in the surface layer of stoichiometric calcite increased systematically to of 1:1 and with further increasing $(Mg^{2+}/Ca^{2+})_{soln}$ to 3:1. The ratio of 2:1 is not indicated by a change of slope (Figure 2a, b).

Id		Reaction	Data source	
			educt	product
K_1	Calcite to dolomite	$2CaCO_3 + Mg^{2+} = CaMg(CO_3)_2 + Ca^{2+}$	B,H,L	B,H,L
K_2	Calcite to disordered dolomite	$2CaCO_3 + Mg^{2+} = CaMg(CO_3)_2 + Ca^{2+}$	B,H,L	L
K_3	Aragonite to dolomite	$2CaCO_3 + Mg^{2+} = CaMg(CO_3)_2 + Ca^{2+}$	B,H,L	B,H,L
K_4	Aragonite to disordered dolomite	$2CaCO_3 + Mg^{2+} = CaMg(CO_3)_2 + Ca^{2+}$	B,H,L	L
K_5	Calcite to magnesite	$CaCO_3 + Mg^{2+} = MgCO_3 + Ca^{2+}$	B,H,L	B,H,L
K_6	Dolomite to huntite	$2CaMg(CO_3)_2 + Mg^{2+} = CaMg_3(CO_3)_4 + Ca^{2+}$	H,L	H,L
K_7	Disordered dolomite to huntite	$2CaMg(CO_3)_2 + Mg^{2+} = CaMg_3(CO_3)_4 + Ca^{2+}$	L	H,L
K_8	Dolomite to magnesite	$CaMg(CO_3)_2 + Mg^{2+} = 2MgCO_3 + Ca^{2+}$	B,H,L	B,H,L
K_9	Disordered dolomite to magnesite	$CaMg(CO_3)_2 + Mg^{2+} = 2MgCO_3 + Ca^{2+}$	L	B,H,L
K_{10}	Dolomite to nesquehonite	$CaMg(CO_3)_2 + Mg^{2+} + 3H_2O = 2MgCO_3 : 3H_2O + Ca^{2+}$	B,H,L	B,H,L
K_{11}	Disordered dolomite to nesquehonite	$CaMg(CO_3)_2 + Mg^{2+} + 3H_2O = 2MgCO_3 : 3H_2O + Ca^{2+}$	L	B,H,L

Table 2: *Compilation of considered reactions, their Gibbs free energies and the* $\log_{10}({}^{a}Mg^{2+}/{}^{a}Ca^{2+})$ *at equilibrium at 25°C assuming that the activities of the solids approach unity.*

Id		Reaction
K_{12}	Magnesite dissolution	$MgCO_3 + H^+ = Mg^{2+} + HCO_3^-$
K_{13}	Huntite dissolution	$CaMg_3(CO_3)_4 + 4H^+ = Ca^{2+} + 3Mg^{2+} + 4HCO_3^-$
K_{14}	Aragonite dissolution	$CaCO_3 + H^+ = Ca^{2+} + HCO_3^-$
K_{15}	Calcite dissolution	$CaCO_3 + H^+ = Ca^{2+} + HCO_3^-$
K_{16}	Disordered dolomite dissolution	$CaMg(CO_3)_2 + 2H^+ = Ca^{2+} + Mg^{2+} + 2HCO_3^-$

Table 3: *Compilation of mineral dissolution reactions needed to estimate K_i in Table 2 with $i = 2, 4, 7, 9$ and 11.*

The ion exchange at surfaces of single crystals of calcite revealed that only one surface layer was involved in this exchange reaction (Möller and Sastri, 1974).

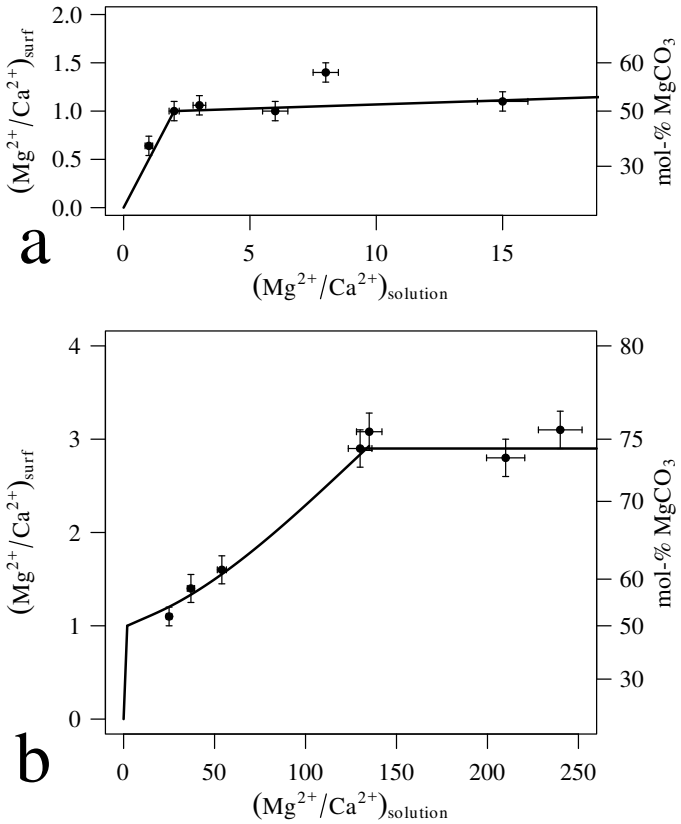

Figure 2: *Surface exchange of Ca^{2+} against Mg^{2+} in the monomolecular surface layer calcite (a; b). Data are taken from Möller (1973); Möller and Sastri (1974).*

Mg^{2+} has a strong tendency to replace Ca^{2+} because the former is more strongly bound in the calcite surface than the latter (Möller, 1973). In presence of Mg^{2+}, the Ca^{2+} concentration increases in solution. The negative logarithm of the ion activity product, $p(IAP)_{Cc_y}$, decreases with increasing Mg^{2+}/Ca^{2+} in calcite surface (Figure 3). For calcite with surface composition between 0 and 50 mol-% $MgCO_3$ $p(IAP)_{Cc_y}$ at 25 °C and atmospheric CO_2 decreases from 8.4 (Plummer and Mackenzie, 1974) to 8.2. For comparison, ordered dolomite ($Ca_{0.5}Mg_{0.5}CO_3$) in 0.1 M NaCl solution, atmospheric CO_2 at 25 °C shows $0.5p(IAP)_{dol}$ of 8.6 (Bénézéth et al., 2018) which is more than that of the dolomitic-composed calcite surface of 8.2.

After reaching the surface composition of 50 mol% $MgCO_3$, $p(IAP)_{Cc_y}$ increases toward the

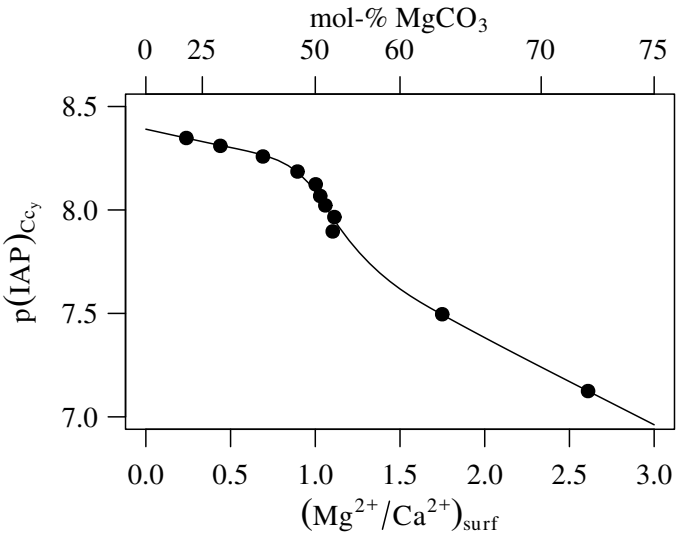

Figure 3: *Estimated ion activity product,* $p(IAP)_{Cc_y}$*, of pure calcite as a function of* Mg^{2+}/Ca^{2+} *surface composition after Koss and Möller (1974).*

huntitic surface composition of calcite ($Mg_{0.75}Ca_{0.25}CO_3$) at Mg^{2+}/Ca^{2+} at about 250 (Figure 2) the estimated ion activity product $p(IAP)_{Cc_y}$ decrease to about 7.0. This decrease in $p(IAP)_{Cc_y}$ is only observed for ion exchange of Mg^{2+} against Ca^{2+} in calcite surfaces. In the exchange Fe^{2+}, Co^{2+} and Ni^{2+} against Ca^{2+} the corresponding $p(IAP)_{Cc_y}$ values increase (Koss and Möller, 1974). The thickness of the surface layer involved in ion exchange is restricted to a one molecular layer as proved by experiments on single crystals (Möller and Sastri, 1974). This result contrasts those of X-ray photoelectron spectrometry which only allow the determination of the average composition of surface layers of 80 to 100 Å thickness equaling about 20 to 25 layers of carbonates. These data represent the composition of the underlying carbonate and do not justify the conclusion of Prokovsky and Schott (2001) that the surface composition of dolomite stays constant in experiments with varying Ca^{2+} and Mg^{2+} concentrations do not change.

As a consequence of the ion exchange of Mg^{2+} against Ca^{2+} the adjacent planar CO_3^{2-} ions rotate accommodating the smaller Mg^{2+} ion (Figure 4). The surface-bound Mg^{2+} shows a lower enthalpy than its Ca^{2+} counterpart (Möller and Rajagopalan, 1976) and the surface exchange of Mg^{2+} against Ca^{2+} spontaneously occurs with loss of free energy. The initial, probably statistical distribution of Mg^{2+} in the surface rearrange into a systematic one, in which the separate alignment of Mg^{2+} and Ca^{2+} ion is energetically favoured. The surface probably displays a mosaic structure of a 2-dimensional dolomitic layer.

3.2 Low-temperature dependence of carbonate equilibria

Groundwater and brines originating from both various lithologies and locations (Table 4) are grouped with respect to their lithological sources such as the Arabian platform carbonates (Figure 5a,b), platform carbonates with local cover of alkali olivine basalts (Figure 5c), and miscellaneous sources such as Pleistocene sediments in northern Germany, springs and wells in the Hauran Plateau/Syria (Cretaceous limestones covered by basalts) and springs discharging from the sediments of the Altiplano/Chile (Figure 5d). The chemical analyses of groundwater and brines are also shown in Appendix A together with the activities of Mg^{2+} and Ca^{2+}, estimated by PHREEQC applying the "llnl.dat" and "pitzer.dat" in PHREEQC (Appelo et al.,

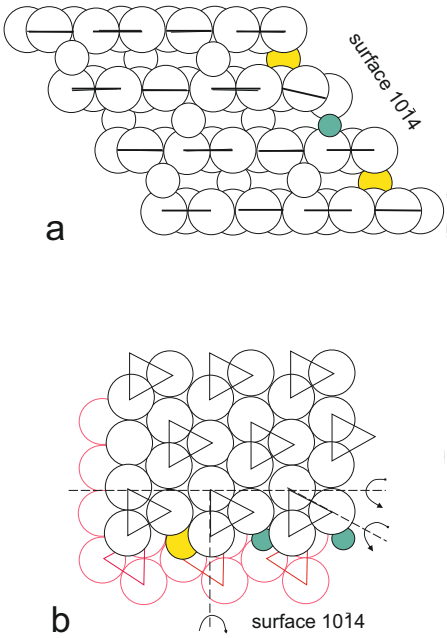

Figure 4: *Schematic cross section (a) and view onto a carbonate plain of calcite (b) showing the structural changes following the exchange of* Ca^{2+} *against* Mg^{2+} *in calcite surface after Möller and Rajagopalan (1972).*

2014).

The change of Mg-Cl brine of the Ha'On well to Ca-Cl brine at Tiberias, both localities being separated by Lake Tiberias, Israel, is of particular interest (Figure 5a). Their Na^+/Cl^- and Br^-/Cl^- are very similar in both types of brines and resemble evaporated seawater (Möller et al., 2012). The Ha'On water samples originate from Cretaceous limestone aquifers that were infiltrated by Late Tertiary evaporated seawater (Möller et al., 2018). Its $\log_{10}({}^{a}Mg^{2+}/{}^{a}Ca^{2+})_{soln}$ value plot near to the equilibrium of disordered dolomite and calcite (after Helgeson et al., 1981). With $(Mg^{2+}/Ca^{2+})_{soln}$ of 2.6, the calcite surface has a dolomitic composition (Figure 2a) but the mineral dolomite has not to be present because of the low temperature of this brine. This dolomitic surface composition mimics the presence of disordered dolomite.

The Tiberias Hot Springs' (THS) brines originate from Jurassic/Cretaceous carbonate aquifers consisting of dolomite and limestone. The lower $\log_{10}({}^{a}Mg^{2+}/{}^{a}Ca^{2+})_{soln}$ than in Ha'On brine is the result of dolomitization of limestone by which Mg^{2+} is consumed and Ca^{2+} is released. The necessary, enhanced temperature to overcome the activation energy of dehydration of Mg^{2+} was supplied by abundant fissures and dykes of olivine basalts in these carbonate rocks. This interpretation is in agreement with PHREEQC inverse modelling (Möller et al., 2012). The final $(Mg^{2+}/Ca^{2+})_{soln}$ of 0.32 indicate similar surface activities of dolomite and calcite. Calcite shows $(Mg^{2+}/Ca^{2+})_{surf}$ of 0.16 (Figure 2a). The dolomite surface is suspected to show $(Mg^{2+}/Ca^{2+})_{surf} > 1$. This example reveals that $(Mg^{2+}/Ca^{2+})_{soln}$ of carbonates solely depends on their surface composition and not on the bulk composition of minerals. The $\log_{10}({}^{a}Mg^{2+}/{}^{a}Ca^{2+})_{soln}$ do not allow identification of carbonate minerals involved by means of thermodynamic considerations. Although here only the influence of Mg^{2+} in solutions is discussed, it should be mentioned that also Fe^{2+} and many other inorganic and organic species vary the solubility of calcite under reducing conditions (Koss and Möller, 1974; Prokovsky et al.,

2009a).

The groundwater of the Hauran Plateau in Syria originate from springs discharging from the alkaline olivine basaltic cover or is exploited from the underlying Cretaceous limestones. The spring water shows lower $\log_{10}({}^{a}Mg^{2+}/{}^{a}Ca^{2+})_{soln}$ than the water from the limestone aquifer because the top basalts have lost its olivine already by weathering. This is different for the deep basalts, where weathering of olivine is still going on. These waters also infiltrate the underlying limestones, whereby high $\log_{10}({}^{a}Mg^{2+}/{}^{a}Ca^{2+})_{soln}$ values are established. The interaction of the Mg^{2+}-rich water from the top of limestones reduces the Mg^{2+} concentration due to surface exchange of Ca^{2+} against Mg^{2+}. Similar trend is to be seen in the low-temperature water from the Golan and Ajloun, where rain water infiltrates through basaltic rocks into underlying Cretaceous limestones. Weathering solution of siliceous rocks or sediments show a wide spread in $\log_{10}({}^{a}Mg^{2+}/{}^{a}Ca^{2+})_{soln}$ (Figure 5d). Ca^{2+} is largely determined by calcite precipitation. Mg^{2+} in such solutions depends on reactions in which Mg^{2+} is involved such as the formation of clay minerals.

In general the spread of temperature-dependent $\log_{10}({}^{a}Mg^{2+}/{}^{a}Ca^{2+})_{soln}$ of these groundwaters and brines plots between -1 and +1, which corresponds up to about 50 mol-% $MgCO_3$ in calcite surfaces (Figure 2). The majority of samples plot below $\log_{10}({}^{a}Mg^{2+}/{}^{a}Ca^{2+})$ of zero thereby indicating surface compositions of calcite up to 40 mol-% of $MgCO_3$. Although the behaviour of magnesian calcite with respect to surface ion exchange of Ca^{2+} against Mg^{2+} has not been studied, it may be suspected that $\log_{10}({}^{a}Mg^{2+}/{}^{a}Ca^{2+})_{soln}$ of magnesian calcite resembles those determined for the $Mg^{2+}-Ca^{2+}$ surface compounds on pure calcite as it will be shown later for ordered dolomite and the dolomitic surface composition on a calcite matrix (subsection 3.3). Here it should be noted that there is not much difference between concentration and activity ratios (Appendix A, Figure A.1). $\text{Log}_{10}({}^{a}Mg^{2+}/{}^{a}Ca^{2+})_{soln}>0$ typify either weathering solutions from Mg^{2+}-rich igneous rocks or Mg^{2+}-rich evaporation brines such as the brines of the Dead Sea, Rift and Ha'On well (Figure 5a) or some of the well waters from the Hauran Plateau/Syria (Figure 5c), and few samples in Figure 5d. $\text{Log}_{10}({}^{a}Mg^{2+}/{}^{a}Ca^{2+})_{soln}$ below $K_{1,HH}$ characterise liquids interacting with Mg-poor rocks such as amphibolites (e.g., KTB-VB; Möller et al., 2005). With few exceptions waters and brines plot between $K_{1,HH}$ and $K_{2,HH}$, most of them between $K_{2,LB}$ and $K_{1,LB}$ mimicking the presence of either ordered or disordered dolomite and HMC. At low temperatures, these phases cannot form but are represented by corresponding surface compositions of calcite. Note that the $\log_{10}({}^{a}Mg^{2+}/{}^{a}Ca^{2+})_{soln}$ rarely plot along the thermodynamical estimated trends. The majority of samples plot along curves subparallel to the given ones indicating abundant Mg^{2+}/Ca^{2+} values.

Groundwater and brines from the same region show temperature-dependent trends of $\log_{10}({}^{a}Mg^{2+}/{}^{a}Ca^{2+})_{soln}$ similar to those suggested by thermodynamic estimates (Figure 5a: Red Sea; Figure 5b: Meizar wells; Figure 5d: Mississippi Salt dome basin). Their $\log_{10}({}^{a}Mg^{2+}/{}^{a}Ca^{2+})_{soln}$ at a given temperature may be different due to environmental conditions and presence of siliceous rocks or sediments from which Mg^{2+} is either gained or consumed.

3.3 Temperature-dependent dissolution of dolomite

Dolomite dissolution experiments reported by Bénezéth et al. (2018) refer to about 3 g of freshly broken dolomite crystals of the composition $Ca_{1.04}Mg_{0.96}(CO_3)_2$ in 100 ml of 0.1 M NaCl solution. The incongruent dissolution of dolomite leads to solutions saturated with respect to calcite and $\log_{10}({}^{a}Mg^{2+}/{}^{a}Ca^{2+})_{soln}$ in equilibrium with the surface composition of both mineral phases dolomite and calcite. The amount of dolomite dissolving depends on the amount of solution. The resulting Mg^{2+} concentration in solution is independent on the amount of solution. Ca^{2+} increases in solution until precipitation of calcite; thereafter its concentration is constant.

Fig	Sources of water/brines	Lithology	Reference
5a	Jordan-Dead Sea Rift/ Israel		
	Ha'On well	Cretaceous limestones	Möller et al. (2009); Bergelson et al. (1999)
	Tiberias Hot Springs	Cretaceous limestones/dolostones	"
	Dead Sea	"	Krumgalz (1997)
	Red Sea Graben Brines	Oceanic basalts; metalliferous sediments	Pierret et al. (2001)
5b	Yarmouk Gorge/Israel, Jordan		
	Springs at Hammat Gader, Israel	Limestones	Siebert et al. (2014, in prep.)
	Mezar well field, Israel	Limestones	"
	Ain Himma, Jordan	Limestones	"
	Mukheibeh Well Field, Jordan	Limestones	"
5c	Yarmouk basin		
	Wells in the Ajloun, Jordan	Limestones and basalts	Siebert et al. (2014)
	Well in the Golan Heights	Limestones and basalts	"
	Springs in the Hauran Plateau, Syria	Mainly basalts	Kattan (1995)
	Wells in the Hauran Plateau, Syria	Cretaceous limestones	Kattan (1995)
5d	Sedimentary rocks containing carbonates		
	North German Basin	Pleistocene sediments	Tesmer et al. (2007); Möller et al. (2008)
	Bohemian Massif	Metagabbros and amphibolites	Paces et al. (1972, 1987)
	Springs of the Altiplano, Chile	Sedimants and acid volcanism	Morteani et al. (2014)
	Mississippi Salt Dome Basin, USA	Granite, granodiorites, amphibolites, phyllites, sst	Kharaka et al. (1987)

Table 4: *Information on groundwaters and brines plotted in Figure 5.*

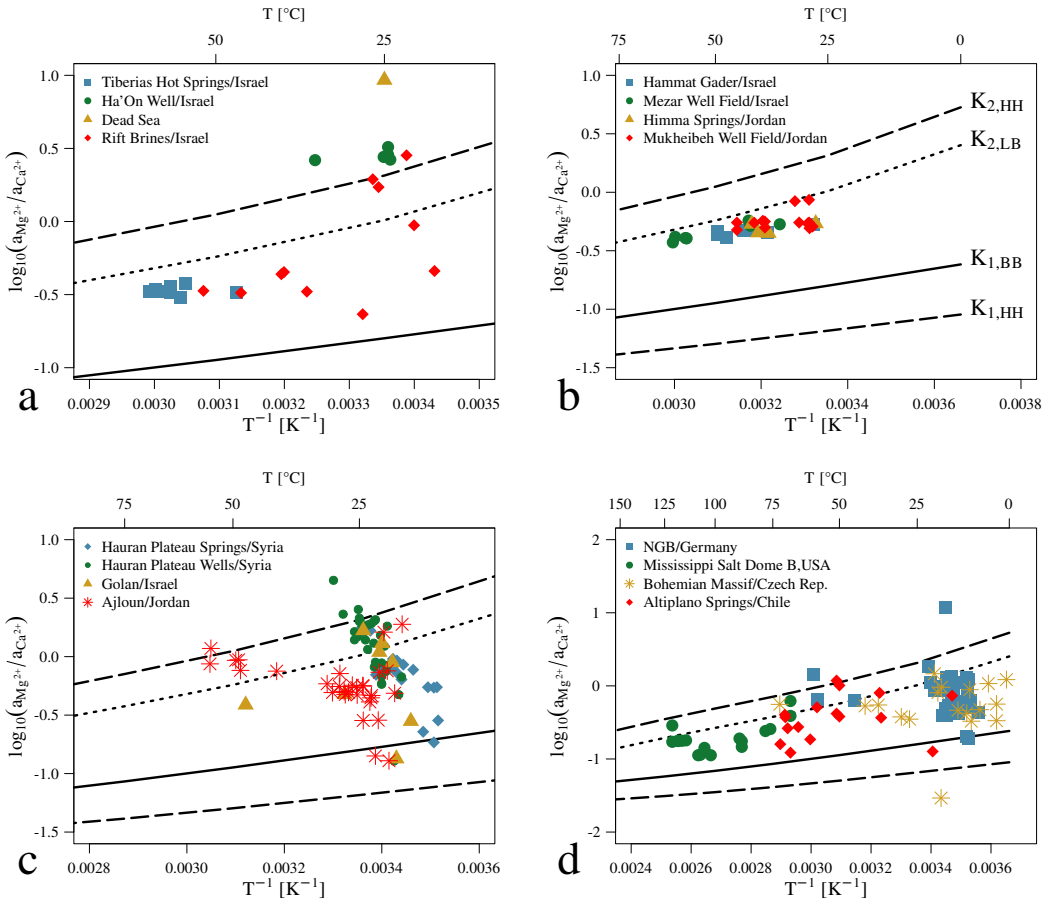

Figure 5: $\mathrm{Log}_{10}({}^{a}\mathrm{Mg}^{2+}/{}^{a}\mathrm{Ca}^{2+})_{\mathrm{soln}}$ *as function of inverse absolute temperature. Average lithologies and sources of analyses are compiled in Table 2. (a) Brines from the Jordan Dead Sea Rift and the Red Sea Graben. Comparison of* $\log_{10}({}^{a}\mathrm{Mg}^{2+}/{}^{a}\mathrm{Ca}^{2+})_{\mathrm{soln}}$ *of Isreali brines from Ha'On well and Tiberias Hot Springs both being related to evaporation of seawater. For more details refer to subsection 3.2. Note that brines with* $\log_{10}({}^{a}\mathrm{Mg}^{2+}/{}^{a}\mathrm{Ca}^{2+})_{\mathrm{soln}} > 0$ *do not form dolomite at the low temperatures of Ha'On and locally in the Rift. Although the environmental conditions in the Rift and the Graben are different,* $\log_{10}({}^{a}\mathrm{Mg}^{2+}/{}^{a}\mathrm{Ca}^{2+})_{\mathrm{soln}}$ *show a similar trend. (b) Groundwater and brines along the Yarmouk Gorge, Israel and Jordan. (c) Groundwater from limestones and basalts overlying the former in the Yarmouk Basin (Isreal, Jordan and Syria). The majority of data plot along a line similar to that in (b). (d) Groundwater and brines from carbonate bearing sediments and sedimentary rocks. Although many reactions other than in limestones are possible, the vertical spread of data is similar to that of (c).* $\mathrm{K}_{1,\mathrm{HH}}$ *and* $\mathrm{K}_{2,\mathrm{HH}}$ *are based on data from Helgeson et al. (1978);* $\mathrm{K}_{1,\mathrm{BB}}$ *results from data of Berman (1988);* $\mathrm{K}_{2,\mathrm{LB}}$ *is estimated from dissolution of disordered dolomite taken from "llnl.data" included in PHREEQC (Appelo et al., 2014) and dissolution of calcite after Berman (1988).*

The extrapolated $\log_{10}(\text{IAP})_{\text{dol}}$ at 25 °C is given by -17.2±0.3. Reevaluation of their reported logarithms of Mg^{2+} and Ca^{2+} concentrations in 0.1 M NaCl solutions of dolomite at various pCO_2 and temperatures between 50 and 250 °C using either "llnl.dat" or "pitzer.dat" yielded $\log_{10}(\text{IAP})_{\text{dol}}$ at 25 °C of -17.8 and -17.5, respectively (Figure 6). For more information refer to Appendix B.

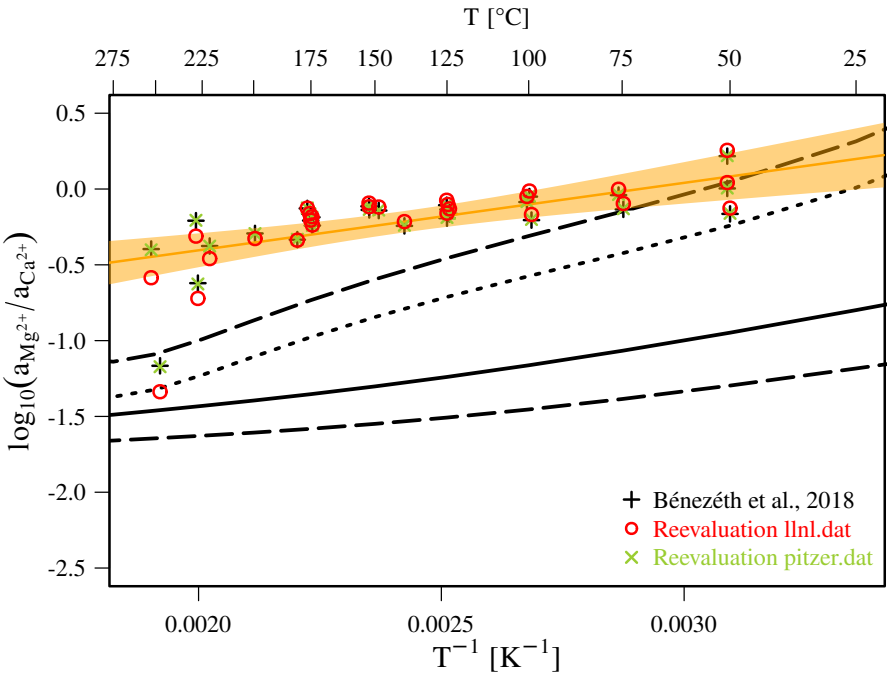

Figure 6: *Comparison of* $\log_{10}({}^{a}Mg^{2+}/{}^{a}Ca^{2+})_{\text{soln}}$ *reported by Bénezéth et al. (2018), their reevaluation by PHREEQC using llnl.dat and pitzer.dat (Appelo et al., 2014) and thermodynamic estimates which are the same as given in Figure 5.*

The incongruent dissolution of dolomite increasing with temperature suggests that Mg^{2+} relative to Ca^{2+} increases in the reactive surface layer of dolomite. The bulk composition of dolomite with 49.8 mol-% $MgCO_3$ did not change during dissolution. Scanning electron micrographs revealed precipitation of calcite and probably dolomite (Bénezéth et al., 2018). Although these solids precipitated, $\log_{10}({}^{a}Mg^{2+}/{}^{a}Ca^{2+})_{\text{soln}}$ decreased from about 0.08 at 50 °C to -0.47 at 250 °C suggesting significant changes of Mg^{2+}/Ca^{2+} in the surface of dolomite. With $Mg^{2+}>Ca^{2+}$ in solution any precipitation of LMC and dolomite increases $(Mg^{2+}/Ca^{2+})_{\text{soln}}$. The incongruent dissolution of dolomite yielding $\log_{10}({}^{a}Mg^{2+}/{}^{a}Ca^{2+})_{\text{soln}}$ of 0.08 at 50 °C (Figure 6) indicates that the surface composition of dolomite has a Mg^{2+}/Ca^{2+} ratio >1. With increasing temperature the difference between the thermodynamic equilibrium of disordered dolomite and calcite and its Mg^{2+}/Ca^{2+} in solution increases which is due to increasing amounts of precipitated LMC. Above about 150 °C the solubility of calcite increases and thus $\log_{10}({}^{a}Mg^{2+}/{}^{a}Ca^{2+})_{\text{soln}}$ decreases. The molar Mg^{2+}/Ca^{2+} surface composition of calcite at 25 °C, however, is 0.6.

In view of Figure 6, the published pIAP values of dolomite refer to the equilibrium of disordered dolomite and calcite, in other words, there is neither congruent dissolution of ordered dolomite nor equilibrium between ordered dolomite and calcite. Although the surfaces of both mineral phases are differently composed, they are in equilibrium with the same Mg^{2+}/Ca^{2+} composition in solution. The $p(\text{IAP})_{\text{dol}}$ =17.2±0.3 after Bénezéth et al. (2018) differs by about

0.8 log units (subsection 3.1) from $p(IAP)_{Cc_y}$ with dolomitic surface composition (2·8.2; Figure 3) but both show the same $\log_{10}({}^{a}Mg^{2+}/{}^{a}Ca^{2+})_{soln}$ values (Figure 7).

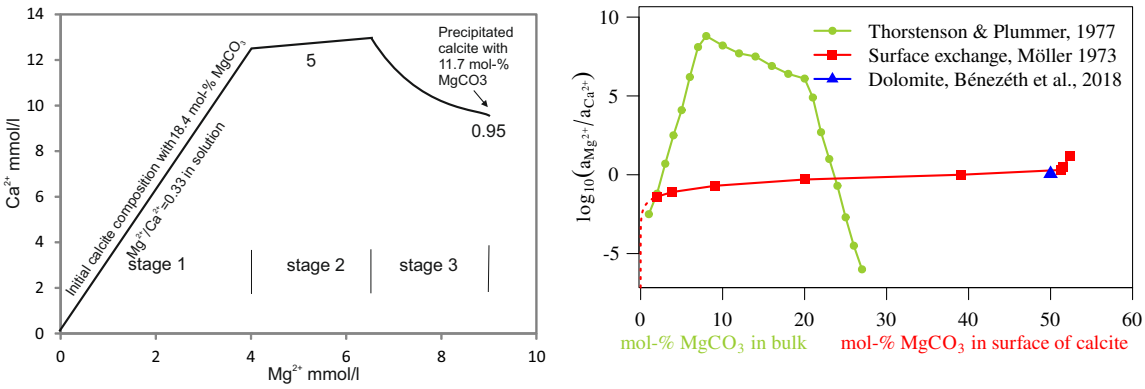

Figure 7: *Dissolution of algae carbonates (HMC). (a) The composite trend is redrawn after Plummer and Mackenzie (1974). Figures below the trend are* Mg^{2+}/Ca^{2+} *values in solution; Beyond the trend initial and final compositions of high magnesium calcite are noted. (b) Comparison of* $\log_{10}({}^{a}Mg^{2+}/{}^{a}Ca^{2+})_{soln}$ *as function of mol-%* $MgCO_3$ *of bulk magnesian calcite (Thorstenson and Plummer, 1977) and of calcite surfaces after* Ca^{2+} *exchange against* Mg^{2+} *(Möller and Rajagopalan, 1972).* $Log_{10}({}^{a}Mg^{2+}/{}^{a}Ca^{2+})_{soln}$ *of dolomite at 25 °C is extrapolated from data reported by Bénezéth et al. (2018).*

Considering IAP of disordered dolomite and calcite the equilibrium between the two is given by eqs. (5) to (7).

The difference of IAP of disordered dolomite and magnesian calcite is derived from Equation 5 and Equation 6, resulting in Equation 7. For ${}^{a}Mg^{2+}/{}^{a}Ca^{2+}=1$, the first term on the right hand site of Equation 7 is zero and thus the difference of the log(IAP) values equals the difference of $\log_{10}\{{}^{a}dol_x\}$ and $\log_{10}\{{}^{a}Cc_y\}^2$.

$$IAP_{dol_x} = {}^{a}(Ca^{2+})^{1+x} \cdot {}^{a}(Mg^{2+})^{1-x} \cdot {}^{a}(CO_3^{2-})^2/\{{}^{a}dol_x\} \tag{5}$$

$$IAP_{Cc_y} = ({}^{a}Ca^{2+})^{1-y} \cdot {}^{a}(Mg^{2+})^{y} \cdot ({}^{a}CO_3^{2-})/\{{}^{a}Cc_y\} \tag{6}$$

$$\log_{10}(IAP_{dol_x}) - 2\log_{10}(IAP_{Cc_y}) = (x-2y)\log_{10}\frac{{}^{a}Mg^{2+}}{{}^{a}Ca^{2+}} + \log_{10}\frac{\{{}^{a}Cc_y\}^2}{\{{}^{a}dol_x\}} \tag{7}$$

Now, $\log(IAP_{Cc_y})$ is known as a function of surface composition of calcite (from Figure 3) and its value is -8.3 for ${}^{a}Mg^{2+}/{}^{a}Ca^{2+}=1$ at 25 °C and 1 bar. Assuming the value of $\{{}^{a}dol_x\}/\{{}^{a}Cc_y^2\}$ is 1, from Equation 7 it is possible to calculate the value of $\log IAP_{dol_x}$:

$$\log(IAP_{dol_x}) - 2\log(IAP_{Cc_y}) = 0 \tag{8}$$

Comparing these results with those of the stoichiometric mineral composition of -17.2±0.3 and -8.45 for dolomite and calcite, it can be assumed that the increase of solubilities of the surface phases are much higher for disordered dolomite (*i.e.*, -8.3·2+17.2=0.6) than for the magnesian calcite (*i.e.*, -8.3+8.45=0.15). The value of -8.3 for magnesium calcite is taken from Figure 3.

From the above reasoning it follows that the solubility of dolomite depends on volume of solution and surface area of both minerals and thereby indirectly on the masses of the two minerals. This is evident from the following estimates. Consider LMC with 1 m^2 surface in

equilibrium with dolomite. Its surface exposes about 1 $m^2/(18 \cdot 10^{-20} \times 6.023 \cdot 10^{23}) = 8.3 \times 10^{-6}$ mol XCO_3 in the surface. If 20 % are $MgCO_3$, the amount of Mg^{2+} bound in the surface equals 1.7 μmol. This amount should be compared with the concentration in solution of about 1 mmol Mg^{2+}/l (Bénezéth et al., 2018). If the volume of solution is only 100 ml, the surface bond Mg^{2+} is about 1% of the released Mg^{2+} from the dolomite. Thus the influence of surface ion exchange is within the analytical uncertainty of Mg^{2+} concentrations.

3.4 Dissolution of high-magnesian calcite

Plummer and Mackenzie (1974) purported the dissolution kinetics of high magnesium calcite (HMC) of algae. The dissolution of HMC with a mean bulk composition of 18.4 mol-% $MgCO_3$ proceed through three stages (Figure 7a). They were related to three different reactions with different rates: (stage 1) congruent dissolution, (stage 2) calcite growth on grain surfaces, whereas Ca^{2+} and Mg^{2+} are still released, and (stage 3) formation of incongruent Mg-calcite precipitate from solution. The reported final $^{a}Mg^{2+}/^{a}Ca^{2+}$ value in solution of steps 1, 2 and 3 increases from 0.3, 0.5 and finally to 0.95, respectively. Part of HMC with initial 18.4 mol-% $MgCO_3$ changes into final precipitate with 11.7 mol-% $MgCO_3$. In stage 3 equilibrium is not reached even after 670 hours. The final solution, however, requests a surface composition of about 30 mol-% $MgCO_3$ (Figure 2a) of the algae HMC and the precipitated LMC, assuming that the surface of the algae HMC behaves similarly to pure LMC. In this case the surfaces of both minerals are higher in mol-% $MgCO_3$ than the average composition of the initial HMC of the algae. Thus, Mg^{2+} is still released from the bulk HMC during crystallization of LMC, although the surface seems to be higher in $MgCO_3$ than the bulk of the algae HMC. Considering surface ion exchange we would explain the whole process differently:

Stage 1: rapid incongruent dissolution, followed by

Stage 2: slowed-down incongruent dissolution of HMC associated with still increasing mol-% $MgCO_3$ of the surface and slightly increasing $(Mg^{2+}/Ca^{2+})_{soln}$, and

Stage 3: slow recrystallization during which bulk Mg^{2+} is still exchanged against Ca^{2+} from solution i.e., the amounts of Mg^{2+} increasing in solution equals the amount of Ca^{2+} decreasing in solution.

Thorstenson and Plummer (1977) derived $\log_{10}(^{a}Mg^{2+}/^{a}Ca^{2+})_{soln}$ based on the composition of HMC and thermodynamic data reported by Plummer and Mackenzie (1974) (Figure 7b). These $\log_{10}(^{a}Mg^{2+}/^{a}Ca^{2+})_{soln}$ data cover a range of 14 orders of magnitude and seems to be unrealistic in view of rapid exchange of Mg^{2+} against Ca^{2+} in calcite surfaces which is proved by very similar $\log_{10}(^{a}Mg^{2+}/^{a}Ca^{2+})$ dissolution data of "dolomite" (Bénezéth et al., 2018) and dolomitic surface of calcite (Figure 7b).

In view of ion exchange results in calcite surfaces, it is suggested that similar processes should also occur in the reported dissolution experiment of HMC. In Figure 7a the corresponding data of HMC alteration during equilibration with solution are compared with the surface composition derived from the described experiments. Note that the decrease of Mg^{2+} content in the altered HMC is associated with increasing Mg^{2+}/Ca^{2+} in solution. Increasing Mg^{2+}/Ca^{2+} in solution yields increasing Mg^{2+}/Ca^{2+} in surface layers of the forming magnesian calcite with less mol-% $MgCO_3$ than in the bulk. This leads to the phenomenon that Mg^{2+}/Ca^{2+} in the surface increases, whereas the corresponding surface–near bulk ratio decreases indicating that the bulk ratios of Mg^{2+} and Ca^{2+} cannot attain equilibrium with the surface ratios. Only the surface layer is in equilibrium with the aqueous phase. From this finding it follows that it is impossible to derive the bulk composition of any Ca-Mg carbonate from the composition of its aqueous

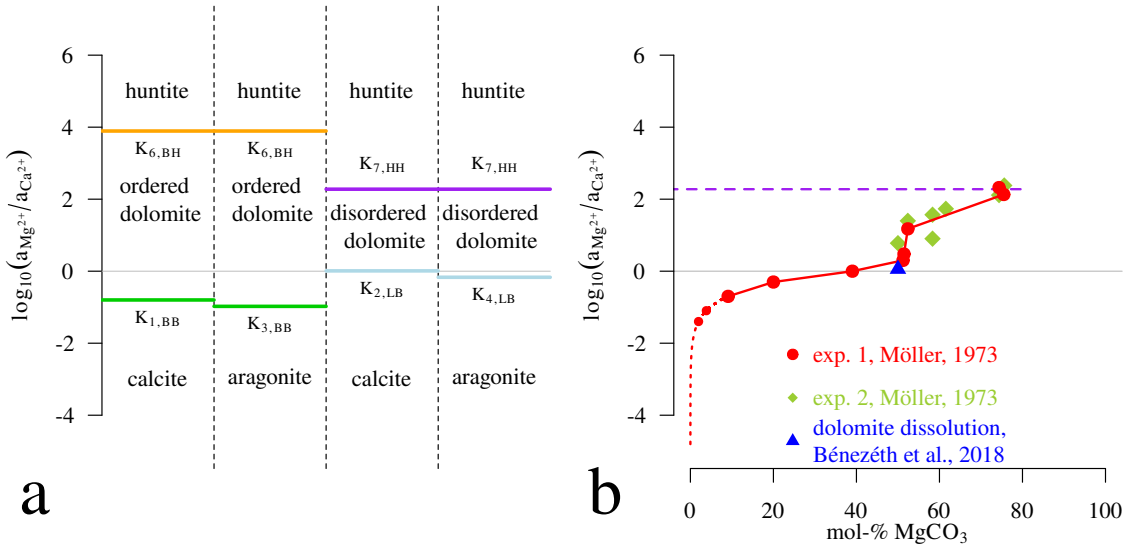

Figure 8: *Comparison of* $\log_{10}({}^{a}Mg^{2+}/{}^{a}Ca^{2+})_{soln}$ *of indicated carbonate mineral equilibria according the thermodynamical estimates (a) and of calcite undergoing surface exchange of* Ca^{2+} *against* Mg^{2+} *in solution (b). The* Mg^{2+} *content in the calcite surface is given in mol-%* $MgCO_3$.

phase because the bulk of the mineral is rarely equilibrated with the ambient solution. It is always the surface that equilibrates with the aqueous phase and that may be quite different from the bulk composition. Even by recrystallization equilibrium between the bulk and surface cannot be attained. $({}^{a}Mg^{2+}/{}^{a}Ca^{2+})_{soln}$ give no hint about the minerals that are involved in the equilibrium.

4 Discussion

Perfect stoichiometry is neither given for calcite nor for dolomite and many other anhydrous carbonate minerals in nature. The apparent thermodynamic ranges of stability of calcite, aragonite, dolomite, and huntite at 25 °C are given by $\log_{10}({}^{a}Mg^{2+}/{}^{a}Ca^{2+})$ in Figure 8a. In detail the relations are much more complex. From bottom to top the formation of magnesian calcite or aragonite depends on Mg^{2+} concentrations. Aragonite only precipitates from Ca^{2+}-HCO_3^- solution containing several g/l of $MgCl_2$ (Kitano et al., 1962). In the Dead Sea aragonite forms at the expense of flushed-in calcite (Barkan et al., 2001). The disordered dolomite and HMC only form during diagenesis or by biogenic processes at significant lower temperatures than ordered dolomite. Disordered dolomite displays a smaller range than dolomite in Figure 8a. Other aspects are that only magnesian calcite with less than 4 mol-% $MgCO_3$ (LMC) precipitates inorganically and the biogenic HMC is thermodynamically metastable but long lived. Next to dolomite, huntite is expected to form but nesquihonite precipitates at both low temperatures and water activity (Davies and Bubela, 1973; Zachmann et al., 1989). The final step would be magnesite, which however is a hydrothermal product (Zachmann et al., 1989).

Contrasting the above sequence, magnesian calcite covers the whole range of calcite to huntite by its adjustable surface composition (Figure 8b). Its $\log_{10}({}^{a}Mg^{2+}/{}^{a}Ca^{2+})_{soln}$ as a function of

mol-% of $MgCO_3$ in the surface of calcite starts at very low values and increases to values of 2.3 in solution, i.e., huntitic surface composition of 0.75 mol-% $MgCO_3$. The corresponding $\log_{10}({}^{a}Mg^{2+}/{}^{a}Ca^{2+})_{soln}$ ratio is seemingly in agreement with the thermodynamic equilibrium of huntite (probably with disordered surface composition) and disordered dolomite and calcite at 25°C (Figure 8b). This corresponds to the behaviour of dolomite dissolution, if disordered dolomite and not ordered dolomite is considered at equilibrium with LMC.

Involvement of the bulk of minerals in equilibria would requests a high mobility of ions in the carbonate lattices. Self-diffusion experiments of ^{45}Ca in calcite revealed that even over millions of years the composition of carbonates would not change to any appreciable extent (Brätter et al., 1972). This result is in agreement with the fact that arrangements of various HMC phases and dolomite survive geological periods (Land, 1985).

In nature, however, dolostones and limestones are often part of the same aquifer. Groundwater passing both lithologies will finally show the latest equilibration with carbonate surfaces. Having in mind that surface compositions of magnesian calcite covers the whole range of $\log_{10}({}^{a}Mg^{2+}/{}^{a}Ca^{2+})$ of carbonates in sediments and weathered rocks, one can hardly expect to get precise information on distinct mineral equilibria from the composition of produced low-temperature fluids.

Unfortunately there is no detailed study on the temperature dependence of surface compositions of calcite or dolomite. However, data from Bénezéth et al. (2018) on dolomite dissolution reveal that even at 253°C no match with thermodynamically defined equilibria between both minerals is found. Only at 25°C the thermodynamical equilibria between disordered dolomite and calcite is seemingly established by their adjusted composition of surface layers of ordered dolomite and calcite.

The ion exchange in carbonate surfaces is associated with structural changes in the surface. These compositionally and structurally varied and charged surfaces are the base of the double layer established in solution. For instance, the Stern layer is the response to the interaction of components of the surface layer with opposite charged components in solution forming inner sphere complexes (Van Cappellen et al., 1993). The formation constants of these surface complexes are different for Ca^{2+}, Mg^{2+} and CO_3^{2-} in the surface and their corresponding counterparts in solution. The reported logK values are higher for Ca^{2+} surface complexes than for the corresponding Mg^{2+} species (Prokovsky et al., 2002; Wolthers et al., 2008). The evaluation of logK values of the various reactions forming surface complexes, however did not consider variations in surface composition of minerals. Generalized, the surface composition and structure of incongruently dissolving carbonates such as dolomite, LMC, HMC or congruently dissolving carbonates such as calcite in solutions containing other divalent or trivalent ions are covered with a double layer the composition of which depends on that of the surface and on the ambient conditions such pH, CO_2 and additional components such as Na^+.

5 Conclusion

In this study the results on carbonate equilibria are discussed in view of thermodynamical estimates and experimental results due to changes of surface composition of carbonates in solutions with auxiliary ions at low temperatures. The equilibria between carbonates are described by $\log_{10}({}^{a}Mg^{2+}/{}^{a}Ca^{2+})$. With few exceptions, it turns out that groundwater and brines irrespective to their sources plot between equilibria of either ordered dolomite–calcite or disordered dolomite-calcite. All these equilibria are controlled by exchange of Ca^{2+} against Mg^{2+} (and possibly other auxiliary ions; Koss and Möller, 1974; Prokovsky and Schott, 2001). Surface compositions of up to 75 mol-% $MgCO_3$ are easily achieved by calcite surfaces, thereby compositionally covering the range of carbonate minerals between calcite/aragonite and huntite.

$\mathrm{Log}_{10}({}^{a}\mathrm{Mg}^{2+}/{}^{a}\mathrm{Ca}^{2+})$ of brines and groundwater from various siliceous and carbonaceous lithologies show a spread from -4 up to 1.5.

In dissolution of HMC, Mg^{2+} content in the altered HMC decreases in association with increasing $\mathrm{Mg}^{2+}/\mathrm{Ca}^{2+}$ in solution. Increasing $\mathrm{Mg}^{2+}/\mathrm{Ca}^{2+}$ in solution leads to increasing $\mathrm{Mg}^{2+}/\mathrm{Ca}^{2+}$ in surface layers of the forming magnesian calcite with less mol-% MgCO_3 than in the bulk. This leads to the phenomenon that $\mathrm{Mg}^{2+}/\mathrm{Ca}^{2+}$ in the surface increases, whereas simultaneously the corresponding surface–near bulk ratio decreases. Only the surface layer is in equilibrium with the aqueous phase indicating that it is impossible to derive the solubility of Ca-Mg carbonates from the composition of their aqueous phases because the bulk of the mineral is rarely equilibrated with the ambient solution. Even during recrystallization equilibrium between the bulk and varying surface composition cannot be attained. In nature the bulk of carbonate minerals never equilibrate with their ambient solutions due to extremely low diffusion of ions in the carbonate lattice.

The assumed incongruent dissolution of dolomite turned out as equilibrium of disordered dolomite and calcite, in other words, there is neither congruent dissolution of ordered dolomite nor equilibrium between ordered dolomite with calcite. In equilibrium, the solubility of the surface composition of disordered dolomite and magnesian calcite are the same. Although the $\mathrm{p(IAP)}_{\mathrm{dol}}$=17.2±0.3 differ by about 0.6 log units (cfr. subsection 3.1) from $\mathrm{p(IAP)}_{\mathrm{Cc_y}}$ with dolomitic surface composition (-8.3 · 2; Figure 3), both show the same $\log_{10}({}^{a}\mathrm{Mg}^{2+}/{}^{a}\mathrm{Ca}^{2+})_{\mathrm{soln}}$ ratios. The "dissolution equilibrium" between carbonates is reached when the surface compositions of calcite and dolomite have approached the same activity ratio of Mg^{2+} and Ca^{2+} in solution.

The above results verify that the dissolution of carbonates depends on the composition of the aqueous phase.

References

Andersson MP, Dideriksen K, Sakuma H, Stipp SLS, 2016. Modelling how incorporation of divalent cations affect calcite wettability-implications for biomineralization and oil recovery. Scientific Reports 6:28854; doi:10.1038/srep28854

Appelo CAJ, Parkhurst DL, Post VEA, 2014. Equations for calculating hydrogeochemical reactions of minerals and gases such as CO_2 at high pressures and temperatures. Geochim Cosmochim Acta 125, 49–67

Arvidson RS, MacKenzie FT, 1999. The dolomite problem: Control of precipitation kinetics by temperature and saturation state. Am J Sci 299, 257–288

Baldermann A, Deditius AP, Dietzel M, Fichtner M, Fischer C, Hippler D, Leis A, Baldermann C, Mavromatis V, Stickler CP Strauss H, 2015. The role of bacterial sulfate reduction during dolomite precipitation; Implications from Upper Jurassic platform carbonates. Chem Geol 412, 1-14

Barkan E, Luz B, Lazar B, 2001. Dynamics of carbon dioxide system in the Dead Sea. Geochim Cosmochim Acta 65, 355-368

Bénezéth P, Berninger U-N, Bovet N, Schott J, Oelkers EH, 2018. Experimental determination of the solubility product of dolomite at 50-253 °C. Geochim Cosmochim Acta 224, 262-275

Bergelson G, Nativ R, Bein A, 1999. Salinization and dilution history of ground water discharging into the Sea of Galilee, the Dead Sea Tansform, Israel. Appl Geochem 14, 91-118

Berman RG, Brown TH, 1985. Heat capacity of minerals in the system $Na_2O-K_2O-CaO-MgO-FeO-Fe_2O_3-Al_2O_33-SiO_2-TiO_2-H_2O-CO_2$: representation, estimation, and high temperature extrapolation. Contr Mineral Petrol 89 (2-3), 168-183

Berman RG, 1988. Internally-Consistent Thermodynamic Data for Minerals in the System $Na_2O-K_2O-CaO-MgO-FeO-Fe_2O_3-Al_2O_3-SiO_2-TiO_2-H_2O-CO_2$. J. Petrol. 29, 445-522, doi:10.1093/petrology/29.2.445

Berninger UK, Saldi GD, Jordan G, Schott J, Oelkers EH, 2017. Assessing dolomite surface reactivity at temperatures from 40 to 120 °C by hydrothermal atomic force microscopy. Geochim Cosmochim Acta 199, 130-142

Brätter P, Möller P, Rösick U, 1972. On the equilibrium of coexisting sedimentary carbonates. Earth Planet Sci Lett 14, 50-54

Davies PJ, Bubela B, 1973. The transformation of nesquihonite into hydromagnesite. Chem Geol 12, 289-300

Davis KJ, Dove PM, De Yoreo JJ, 2000. The role of Mg^{2+} as an impurity in calcite growth. Sci 290, 1134-1137

Dick JM, 2008. Calculation of the relative metastabilities of proteins using the CHNOSZ software package, Geochemical Transactions 9:10, doi:10.1186/1467-4866-9-10

Dobberschütz S, Nielsen MR, Sand KK, Civioc R, Bovet N, Stipp SLS, Andersson MP, 2018. The mechanisms of crystal growth inhibition by organic and inorganic inhibitors. Nature Communications, 9 (1):1578, doi:10.1038/s41467-018-04022-0

Generosi J, Ceccato M, Anderson MP, Hassenkam T, Dobberschütz S, Bovet N, Stipp SLS, 2016. Calcite wettability in the presence of dissolved Mg^{2+} and SO_4^{2-}. Energy Fuels 31 (1), 1005-1014, doi:10.1021/acs.energyfuels.6b02029

Gledhill DK, Morse JW 2006. Calcite solubility in Na-Ca-Mg-Cl brines. Chem Geol 233, 249-256

Gregg JM, Sibley DF, 1984. Epigenetic dolomitization and the origin of xenotopic dolomite texture - reply. J Sediment Petrol 54, 908-931

Gregg JM, Bish DL, Kaczmarek SE, Machel HG, 2014. Mineralogy, nucleation and growth of dolomite in the laboratory and sedimentary environment: A review. Sediment 62, 1749–1769

Helgeson HC, Delany JM, Nesbitt HW, Bird DK, 1978. Summary and critique of the thermodynamic properties of rock-forming minerals. Am J Sci 278A, 1-229, http://www.worldcat.org/oclc/13594862

Helgeson HC, Kirkham DH, Flowers GC, 1981. Theoretical prediction of the thermodynamic behavior of aqueous electrolytes at high pressures and temperatures: Calculation of activity coefficients, osmotic coefficients, and apparent molal and standard and relative partial molal properties to 600 °C and 5 kB. Am J Sci 281, 1249-1516

Kattan Z, 1995. Chemical and environmental isotope study of the fissured basalt aquifer system of the Yarmouk basin. IAEA Symposium on isotopes in water resources, Vienna, Austria. IAEA-SM/336/28

Kharaka YK, Maest AS, Carother WW, Law LM, Lamothe PJ, Fries TL, 1987. Geochemistry of metal-rich brines from central Mississippi Salt Dome basin, USA. Appl Geochem 2, 543–561

Kitano Y, Park K, Hood DW, 1962. Pure aragonite synthesis. J Geophys Res 67, 4873-4874

Koss V, Möller P, 1974. Oberflächenzusammensetzung, Löslichkeit und Ionenaktivitätsprodukt von Calcit in fremdionenhaltigen Lösungen. Z Anorg Allg Chem 410, 165-178

Krumgalz BS, 1997. Ion interaction approach to geochemical aspects of the Dead Sea. In: Niemi TM, Ben-Avraham Z, Gat JR (eds). The Dead Sea –The Lake and its setting. Oxford Monograph on Geology and Geophysics 36, New York, Oxford, 145-160

Lakstanov LZ, Belova DA, Ohkrimenko DV, Stipp SLS, 2017. Role of alginate in calcite recrystallization, Crystal Growth & Design 15, 419–427

Land LS, 1985. The origin of massive dolomite. J Geological Education 33, 112–125

Land LS, 1998. Failure to precipitated dolomite at 25 °C from dilute solution despite 1000-fold oversaturation after 32 years. Aquatic Geochem 4, 361–368

Mavromatis V, Gautier Q, Bosc O, Schott J, 2013. Kinetics of Mg partition and Mg stable isotope fractionation during incorporation in calcite. Geochim Cosmochim Acta 114, 188–203

Möller P, 1973. Determination of the composition of surface layers of calcite in solutions containing Mg^{2+}. J Inorg Nucl Chem 35, 395–401

Möller P, Rajagopalan G, 1972. Cationic distribution and structural changes of mixed Mg-Ca layers on calcite crystals. Physik Chem 71, 47-56

Möller P, Rajagopalan G, 1976. Changes of excess free energies in the crystal growth process of calcite and aragonite due to presence of Mg^{2+} ions in solution. Z Physik Chem NF 99, 187–198

Möller P, Sastri CS, 1974. Estimation of the number of surface layers involved in Ca-^{45}Ca isotopic exchange with solution. Z Physik Chem NF 89, 80–87

Möller P, Rosenthal E, Geyer S, 2009. Characterization of aquifer environments by major and minor elements and stable isotopes of sulfate. In: Hoetzl H, Möller P, Rosenthal E (Eds.), The Water of the Jordan Valley. Springer Verlag, Berlin, Heidelberg, pp. 75–121

Möller P, Rosenthal E, Inbar N, Siebert C. 2018. Development of the Inland Sea and its evaporites in the Jordan-Dead Sea transform based on hydrogeochemical considerations and the geological consequences. Intern J Earth Sci 107, 2409–2433

Möller P, Siebert C, Geyer S, Inbar N, Rosenthal E, Flexer A, Zilberbrand M, 2012. Relationship of brines in the Kinnarot Basin, Jordan-Dead Sea Rift Valley. Geofluids 12, 166–181

Möller P, Weise SM, Tesmer M, Dulski P, Pekdeger A, Bayer U, Magri F, 2008. Salinization of groundwater in the North German Basin: results from conjoint investigation of major, trace elements and multi-isotopic distribution. Int J Earth Sci 97, 1075–1073

Möller P, Woith H, Dulski P, Lüders V, Erzinger J, Kämpf H, Pekdeger A, Hansen B, Lodemann M, Banks D, 2005. Main and trace elements in KTB-VB fluid: Composition and hints to its origin. Geofluids 5, 28–41

Montanari G, Rodriguez-Blanco JD, Bovet N, Stipp SLS 2017. Impact of citrate ions on the nucleaction and growth of anhydrous CaCO3. Crystal Growth & Design 17, 5269–5275

497 Morteani G, Möller P, Dulski P, Preinfalk C, 2014. Major, trace elements and stable isotope
498 composition of water and muds precipitated from hot springs of Bolivia: Are the waters of
499 the springs potential ore forming fluids? Chem Erde-Geochem 74, 49–62

500 Mucci A, Morse JM, 1983. The incorporation of Mg^{2+} and Sr^{2+} into calcite overgrowths:
501 influences of growth rate and solution composition. Geochim Cosmochim Acta 47, 217-233

502 Nielsen MR, Sand KK, Rodriguez Blanco JD, Bovet NE, Generosi J, Dalby KN et al.
503 Inhibition of calcite growth: combined effects of Mg^{2+} and SO_4^{2-}. Crystal Growth & Design.
504 2016;16(11):6199-6207

505 Paces T, 1972. Chemical characteristics and equilibration in natural water–felsic rock–CO_2
506 systems. Geochim Cosmochim Acta 36, 217–240

507 Paces T, 1987. Hydrochemical evolution of saline waters from crystalline rocks of the Bohemian
508 Massif (Czechoslovakia), in: Fritz P, Frape SK (Eds), Saline water and gases in crystalline
509 rocks. Geol Ass Canada Spec Pap 33, 145–156

510 Perez-Fernandez A, Berninger U-N, Mavromatis V, Pogge von Strandmann PAE, Oelkers EH,
511 2017. Ca and Mg isotope fractionation during the stoichiometric dissolution of dolomite
512 at temperatures from 51 to 126°C and 5 bars CO_2 pressure. Chem Geol 467, 76–88,
513 doi:10.1016/j.chemgeo.2017.07.026.

514 Pierret MC, Clauer N, Bosch D, Blanc G, France-Lanord C, 2001. Chemical and isotopic
515 ($^{87}Sr/^{86}Sr$, $\delta^{18}O$, δD) constraints to the formation processes of Red-Sea Brines. Geochim
516 Cosmochim Acta 65, 1259–1275

517 Plummer LN, Busenberg E, 1982. The solubilities of calcite, aragonite and vaterite
518 in CO_2-H_2O solutions between 0 and 90 °C, and an evaluation of the aqueous
519 model for the system $CaCO_3-CO_2-H_2O$. Geochim Cosmochim Acta 4, 1011–1040.
520 doi:10.1016/0016-7037(82)90056-4

521 Plummer LN, Mackenzie FT, 1974. Predicting mineral solubility from rate data. Application to
522 dissolution of magnesian calcite. Amer J Sci 274, 61–83

523 Prokovsky OS, Schott J, 2001. Kinetics and mechanism of dolomite dissolution in neutral to
524 alkaline solutions revisited. Am J Sci 301, 597–626

525 Prokovsky OS, Schott J, Mielczarski JA, 2002. Surface speciation of dolomite and calcite I
526 aqueous solutions. Encyclopedia of Surface and Colloid Science. Marcel Dekker, Inc, New
527 York, 5081–5095

528 Prokovsky OS, Golubev SV, Schott J, 2005. Dissolution kinetics of calcite, dolomite and
529 magnesite at 25 °C and 0 to 50 atm pCO_2. Chem Geol 217, 239–255

530 Prokovsky OS, Golubev SV, Jordan G, 2009a. Effect of organic and inorganic ligands on calcite
531 and magnesite dissolution rates at 60 °C and 30 atm pCO_2. Chem Geol 265, 33–43

532 Prokovsky OS, Golubev SV, Schott J, Castillo A, 2009b. Calcite, dolomite and magnesite
533 dissolution kinetics in aqueous solutions at acid to circumneutral pH, 25 to 150 °C and 1
534 to 55 atm pCO_2: New constraints in sedimentary basins. Chem Geol 265, 20–32

535 Sastri CS, Möller P, 1974. Study of the influence of Mg^{2+} ions on Ca-^{45}Ca isotope exchange on
536 the surface layer of calcite single crystals. Chem Phys Lett 26, 116–120

Siebert C, Möller P, Geyer S, Kraushaar S., Dulski P, Guttman J, Subah A, Rödiger T, 2014. Thermal water in the Yarmuk Gorge and their relation to surrounding aquifers. Chem Erde-Geochem 74, 425-441

Siebert C, Möller P, Shalev E, Guttmann Y, Rosenthal E, Inbar N, Raggad M, Magri F (in prep.): The confluence of three regional groundwater flows, distinguished by REE+Y and U (VI): the case of the Yarmouk Gorge

Tesmer M, Moeller P, Wieland S, Jahnke C, Voig H, Pekdeger A (2007) Deep reaching fluid flow in the North East German Basin: origin and processes of groundwater salinisation. Hydrogeol J 15, 1291–1306

Thorstenson DC, Plummer LN, 1977. Equilibrium criteria for two-component solids reacting with fixed composition in an aqueous phase- Example: the magnesian calcites. Amer J Sci 277, 1203–1223

Van Cappellen P, Charlet L, Stumm W, Wersin P, 1993. A surface complexation model of the carbonate mineral-aqueous solution interface. Geochim Cosmochim Acta 57, 3505–3518

Wang X, Chou I-M, Hu W, Yuan S, Liu H, Wan Y, Wang X, 2016. Kinetic inhibition of dolomite precipitation; insight from Raman spectroscopy of Mg^{2+}–SO_4^{2-} ion pairing in $MgSO_4/MgCl_2/NaCl$ solutions at temperatures of 25 to 200 °C. Chem Geol 435, 10–21

Warren J, 2000. Dolomite: occurrence, evolution and economically important associations. Earth Sci Rev 52, 1–81

Wolthers M, Charlet L, Van Cappellen P, 2008. The surface chemistry of divalent meta carbonate minerals; A critical assessment of surface charge and potential data using the charge distribution multi-site ion complexation model. Amer J Sci 208, 905–941

Zachmann DW, 1989. Mg-carbonate deposits in freshwater environment, in Möller P (Ed.), Magnesite–geology, mineralogy, geochemistry, formations of Mg-carbonates. Monograph series on ore deposites, Gebrüder Borntraeger Berlin, Stuttgart, 28, 61-94

Appendix A. Relationship between activities and concentrations in Mg^{2+}/Ca^{2+}

All samples displayed in Figure 5 are compiled in an electronic file which can be obtained from the authors on request.

The same samples are plotted together in Figure A.1 separated by their ionic strength of either I<1 (circles) or I>1 (laying crosses). Figure A.1a reveals that ionic strength has little influence on $\log_{10}({}^{a}Mg^{2+}/{}^{a}Ca^{2+})$. Figure A.1b shows that the majority of brines and groundwater plot in the same array. The distribution of $\log_{10}({}^{a}Mg^{2+}/{}^{a}Ca^{2+})_{soln}$ in groundwaters and brines and its temperature dependence suggests that they are dominantly framed by the thermodynamic equilibria of disordered dolomite-calcite and ordered dolomite-calcite.

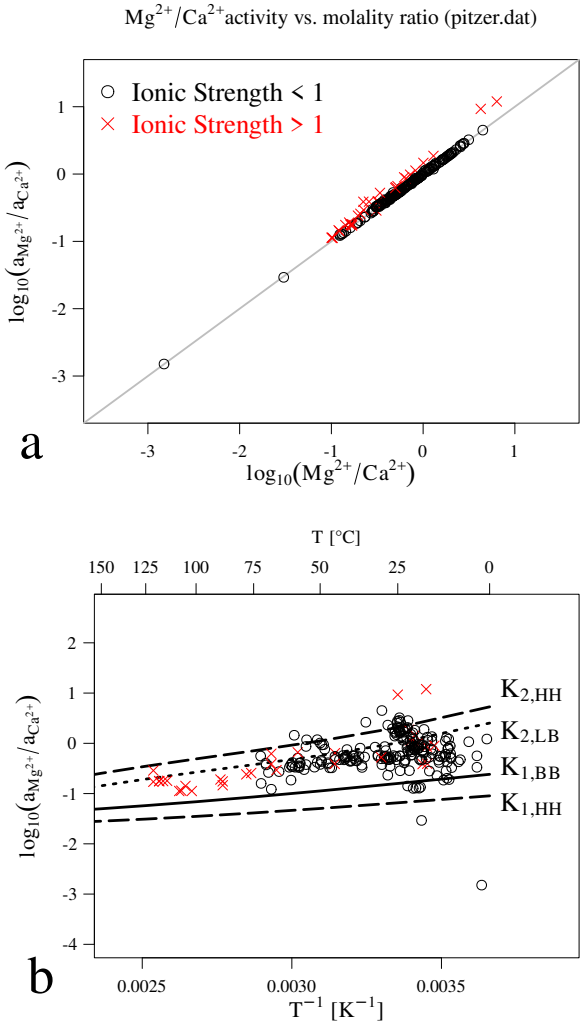

Figure A.1: *Plot of all samples from Figure 5 into an unique diagram but separating the samples according to their ionic strength. Circles and laying crosses represent ionic strength smaller or greater than unity, respectively.* ***(a)*** *Cross plots of activity and concentration ratios in groundwater and brines showing little difference between the two.* ***(b)*** *Cross plots of all samples in Figure 5 showing no systematic differences with respect to ionic strength. The indices of reactions* K_i *are:* $K_{1,HH}$ *and* $K_{2,HH}$ *based on data from Helgeson et al. (1978);* $K_{1,BB}$ *results from data of Berman (1988);* $K_{1,LB}$ *is estimated from dissolution of disordered dolomite taken from PHREEQC's "llnl.dat" and dissolution of calcite after Berman (1988).*

Appendix B. Reevaluation of solubility experiments of Bénezéth et al. (2018)

The experimental results of dolomite dissolution published by Bénezéth et al. (2018) have been reevaluated with the aid of PHREEQC models. The models have been constrained imposing the measured pH, total inorganic carbon, concentrations of Ca^{2+} and Mg^{2+} and by a background salinity of 0.0975 mol/kg Na^{+} and 0.1 mol/kg Cl^{-}. The aim was to determine activities of carbonate CO_3^{2-}, Ca^{2+} and Mg^{2+} following the extended Debye-Hückel and Pitzer activity theories, implemented respectively by the "llnl.dat" and "pitzer.dat" databases. The validity fields of these approaches are reported to be up to 300 °C and ionic strength around 2 mol/kg for NaCl dominated solutions in case of llnl.dat; and up to 200 °C and halite saturation for Pitzer. All data sets are fitted by the same linear model suggested by Bénezéth et al. (2018):

$$\log_{10}\left(\mathrm{IAP}\right)_{\mathrm{dol}} = a + b \cdot (1/T) + c \cdot T$$

with T in Kelvin. These fitted models are displayed as solid lines in Figure B.1a. The speciation calculated by the diverse models result in lower $\log_{10}$(IAP) values of dolomite than -17.2 reported by the original authors, i.e., -17.8 and -17.5. More in detail, the discrepancy can be imputed to the calculated CO_3^{2-} concentrations, which are up to one order of magnitude lower than the reported measured values (Figure B.1b) and to the calculated product of activity coefficients (Figure B.1c).

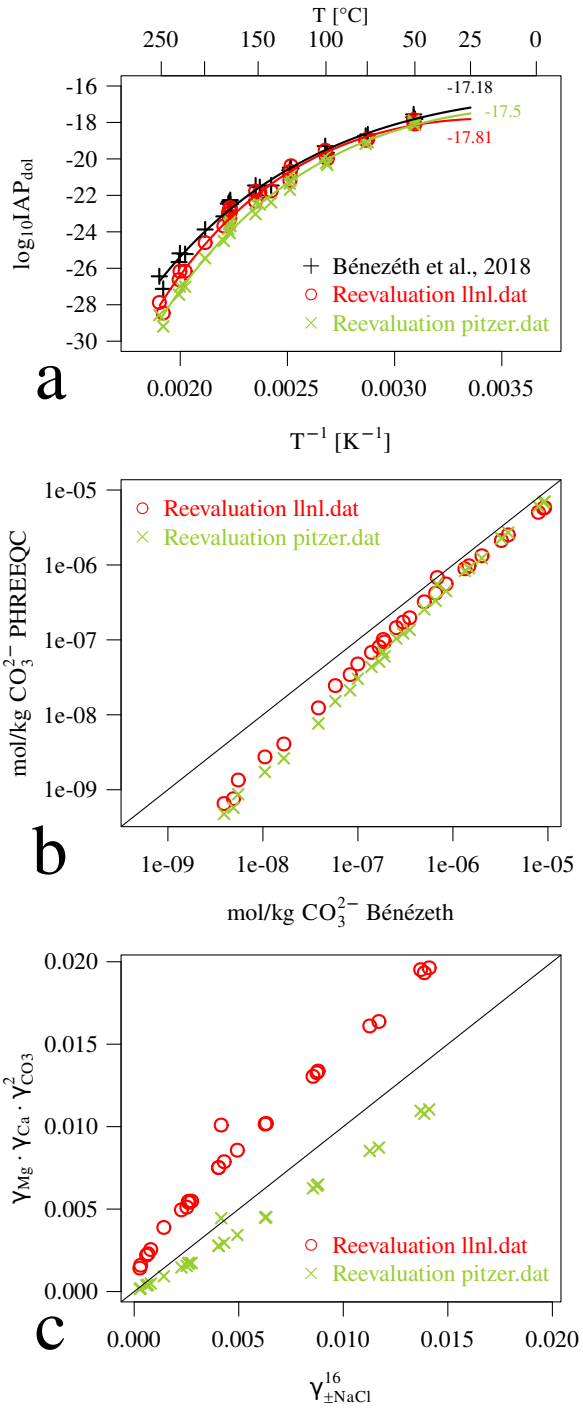

Figure B.1: ***(a)*** *Reevaluation of* $\log_{10}(\mathrm{IAP})_{\mathrm{dol}}$ *by PHREEQC models using the databases llnl.dat and pitzer.dat from the data from Bénezéth et al. (2018);* ***(b)*** *comparison of* CO_3^{2-} *of and reevaluated* CO_3^{2-} *with PHREEQC;* ***(c)*** *the calculated products of activity coefficients according to llnl.dat and pitzer.dat are greater or lower than those used by Bénezéth et al. (2018)*